A. Nominal Bus Model

To model a bus interconnect, we use the *RC* network model found in [16], which is briefly described next. Introduce the matrix $T(s)$ given in Laplace domain by

$$T(s) \triangleq \begin{bmatrix} Y & Z & 0 & \cdots & 0 & 0 \\ Z & X & Z & \cdots & 0 & 0 \\ \vdots & \vdots & \vdots & \vdots & \vdots & \vdots \\ 0 & 0 & 0 & \cdots & X & Z \\ 0 & 0 & 0 & \cdots & Z & Y \end{bmatrix}. \tag{10}$$

Here

$$X = 1 + sR_w(2C_c + C_g) \tag{11}$$
$$Y = 1 + sR_w(C_g + C_c) \tag{12}$$
$$Z = -sR_wC_c \tag{13}$$

where R_w is the interconnect wire resistance, C_g is the interconnect wire-to-substrate capacitance, and C_c is the inter-wire capacitance called the coupling capacitance. These parameters are computed as follows:

$$R_w \triangleq \frac{\rho L}{w_w t_1} \tag{14}$$

$$C_g \triangleq \frac{\epsilon L w_w}{h} \tag{15}$$

$$C_c \triangleq \frac{2\epsilon L t_1}{d}. \tag{16}$$

ρ is the resistivity of copper, w_w is the wire width, d is the separation between two wires, t_1 is the wire height, h is the height of the wire above the substrate, ϵ is the permittivity of the oxide between wires, and L is the length of the interconnect. A short section of the bus (of length L) can be described by the MIMO transfer function matrix

$$H(s) \triangleq T^{-1}(s). \tag{17}$$

The transfer function matrix of longer interconnect is obtained by multiplying transfer function matrices $H(s)$ of shorter interconnects.

The variability of the bus characteristics as seen through the variability of the transfer function matrix $H(s)$ depends on the variability of parasitic parameters R_w, C_g, and C_c. According to [4], in a 0.1-μm technology, these parameters may vary as follows:

$$\rho = \rho \pm \Delta\rho = 2.2 \times 10^{-8} \pm 30\% \ \Omega\text{m} \tag{18}$$
$$d, w_w = (d, w_w) \pm \Delta(d, w_w) = 237 \times 10^{-9} \pm 20\% \ \text{m} \tag{19}$$
$$t_1, h = (t_1, h) \pm \Delta(t_1, h) = 498 \times 10^{-9} \pm 15\% \ \text{m}. \tag{20}$$

To illustrate and better understand how the process variability affects the parasitic parameters R_w, C_g and C_c, Fig. 3 is given which depicts two bus interconnects with parameters that define their geometry. The bus on the right is an ideal interconnect, while one on the left suffers from the erosion. The erosion is one type of process variabilities that occurs in the case of dense array thin interconnects, and it is characterized by the oxide and metal removal. The erosion results in effective decrease of the
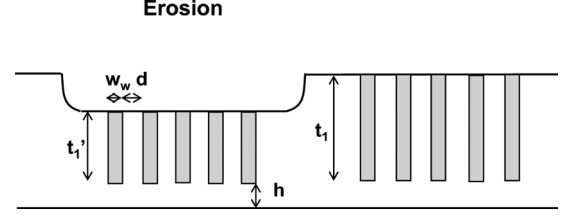
Erosion

Fig. 3. Example of process induced bus variability.

wire height t_1 leading to an increase of the wire resistance R_w and decrease of the coupling capacity C_c. This shows that the process variability can cause correlated variations of the parasitic parameter values. As noted in [4], the examples of parameters' correlations are as follows.

1) Given a fixed wire pitch, the variation of the separation between two wires d is negative of the variation of the wire width w_w.
2) The wire height t_1 and the height of the wire above the substrate h are negatively correlated with a correlation coefficient of -0.5.

The effect of previous correlations are taken into account in the case-study given in Section VI.

B. Compound Bus Model

In this section, we introduce the model which has been widely used in control and information theory to describe the variability in the frequency domain [25]–[27]. The model relies on the H^∞ normed linear space and $\|\cdot\|_\infty$ norm (for precise definitions see the Appendix). The $\|\cdot\|_\infty$ norm is defined by using the singular value decomposition (SVD) of the matrix. In essence, any matrix $H \in \mathbf{C}^{p \times p}$ assumes a decomposition $H = U\Sigma V^H$, where $U \in \mathbf{C}^{p \times p}$ and $V \in \mathbf{C}^{p \times p}$ are unitary matrices, and $\Sigma \in \mathbf{C}^{p \times p}$ is a diagonal matrix with positive entries $\{\sigma_i\}_{i=1}^r$ representing the singular values of H. When H is a transfer function matrix of the communication channel, the entries of Σ can be understood as the attenuation coefficients of the channel, while U and V define the phase. When H is scalar, the analogy is even more clear since the singular value is equivalent to the modulus $|H|$ of the transfer function $H = |H|e^{j\phi_H}$. To understand why the SVD is a natural way to model uncertainty, notice that the Shannon's capacity of communication channels defined by (3) is directly related to the singular values of H [28].

Now, since the manufacturing process variability determines the variability of the bus parasitic parameters such as capacitance and resistance, it determines the variability of the transfer function matrix $H(z)$ and the set of all possible frequency responses $H(e^{j\theta})$ of the bus. Therefore, the model, which takes into account the manufacturing process variability, is the set of all possible transfer function matrices $H(e^{j\theta})$. One way to describe such a set (call it A_2) is to represent it by a ball in the frequency domain by using H^∞ space and $\|\cdot\|_\infty$ norm such as (21), shown at the bottom of the next page. The ball A_2 is centered at a known transfer function $H_{nom}(e^{j\theta})$, the so-called nominal transfer function. The size of the ball is determined by a perturbation $w(e^{j\theta})\Delta(e^{j\theta})$. The perturbation is defined by: 1) an unknown matrix $\Delta(e^{j\theta})$ that takes care of the uncertainty in the
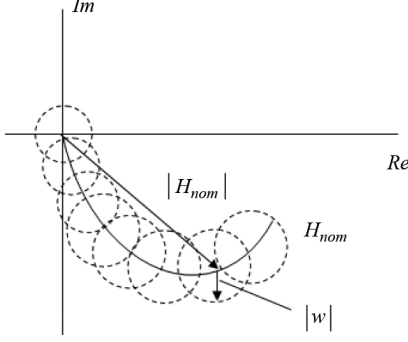
Fig. 4. Nyquist plot of variability modeling.

phase because $\|\Delta\|_\infty \leq 1$ and 2) a known scalar transfer function $w(e^{j\theta})$ that defines A_2 radius. To understand why $w(e^{j\theta})$ defines the radius of the ball A_2 observe that a ball in the complex domain is given by

$$|z - z_0| \leq r, \; z, \; z_0 \in \mathbf{C}. \qquad (22)$$

Since we deal with matrices, to define the ball we need to use matrix maximum singular value $\bar{\sigma}(\cdot)$. Then the ball in the frequency domain is given by

$$\bar{\sigma}(H(e^{j\theta}) - H_{nom}(e^{j\theta})) \leq |w(e^{j\theta})|\bar{\sigma}(\Delta(e^{j\theta}))$$
$$\leq |w(e^{j\theta})|\|\Delta\|_\infty$$
$$\leq |w(e^{j\theta})| \qquad (23)$$

since $\|\Delta\|_\infty = \sup_{\theta \in [0,2\pi)} \bar{\sigma}(\Delta(e^{j\theta})) \leq 1$, and $\bar{\sigma}(AB) \leq \bar{\sigma}(A)\bar{\sigma}(B)$. At each frequency, the size of the set A_2 is determined by the radius $|w(e^{j\theta})|$.

To further clarify this point, we refer to Fig. 4 which shows the Nyquist plot of a scalar transfer function $H_{nom}(e^{j\theta})$. A Nyquist plot is a imaginary part versus real part of a transfer function. Each point on the graph corresponds to one frequency θ. The length of the vector connecting the origin and any point on the graph corresponds to a transfer function modulus (attenuation) at some frequency θ, while the angle between the vector and the positive real line corresponds to a phase. The perturbation superimposes the variability at each frequency by a ball centered at the apex of the vector with the radius determined by $|w(e^{j\theta})|$. Thus, any point within the ball is possible because $\Delta(e^{j\theta})$ has an unknown phase and $|\Delta(e^{j\theta})| \leq 1$. Based on Fig. 4, A_2 can be seen as a tube around $H_{nom}(e^{j\theta})$.

The definition of A_2 also implies

$$\bar{\sigma}(H_{nom}) - |w| \leq \bar{\sigma}(H) \leq \bar{\sigma}(H_{nom}) + |w| \qquad (24)$$

which gives an upper and lower bound on the singular values (attenuation coefficients) of the transfer function matrices that belong to A_2. $H_{nom}(e^{j\theta})$ and $w(e^{j\theta})$ are appropriately chosen

according to (17) to describe all possible matrices $H(e^{j\theta})$. Usually, $H_{nom}(e^{j\theta})$ is determined by the nominal values of the parasitic parameters of the bus, while $|w(e^{j\theta})|$ follows from the parasitic parameters variations.

IV. ACHIEVABLE DATA RATE OF THE BUS

In this section, the formula for computing the achievable data rate is provided for the bus model described by (3) and (21). It is assumed that the transmitted data sequence $\{x(t)\}_{t \geq 0}$ is random as it is in reality. First, the definition of power constraint for random signals is introduced. Second, the formula for the achievable data rate is given by the maximin optimization problem where the objective function is the mutual information (MI) rate. Third, the solution of the maximin optimization problem is presented and the implications of solution are discussed.

A. Power Constraint for Random Signals

Since we deal with the random signals, the power constraint equivalent to (2) should be introduced. It is given in terms of the power spectral density (PSD) matrix of $x(t)$ denoted by $W_\mathbf{x}(\theta)$. PSD $W_\mathbf{x}(\theta)$ is related to its correlation function $R(k)$ through the inverse Fourier transform in the following way:

$$R(k) \triangleq E[x(t+k)x^H(t)] \triangleq \frac{1}{2\pi}\int_0^{2\pi} W_\mathbf{x}(\theta)e^{j\theta k}d\theta \quad (25)$$

or for $k = 0$

$$R(0) \triangleq E[x(t)x^H(t)] \triangleq \frac{1}{2\pi}\int_0^{2\pi} W_\mathbf{x}(\theta)d\theta. \qquad (26)$$

Then, the power constraint is given by the set of PSD matrices

$$A_1 \triangleq$$
$$\left\{ W_\mathbf{x}(\theta) : \mathrm{Trace}E[x(t)x^H(t)] = \int_0^{2\pi} \mathrm{Trace}(W_\mathbf{x}(\theta))d\theta \leq P \right\}. \qquad (27)$$

It is clear that

$$\mathrm{Trace}E[x(t)x^H(t)] = \sum_{i=1}^m E[x_i^2(t)] \qquad (28)$$

represents the average power of the transmitted data over all p bus interconnects.

B. Achievable Rate

The achievable rate subject to variability in the transfer function matrix $H(e^{j\theta})$ described by (21) is going to be related to the MI rate. A nice property of the MI rate formula used here is that it is given in the frequency domain. This enables us to use a frequency domain variability description, which is of a great practical importance. On the other hand, it should be observed that

$$A_2 \triangleq \left\{ H(e^{j\theta}) \in H^\infty : H(e^{j\theta}) = H_{nom}(e^{j\theta}) + w(e^{j\theta})\Delta(e^{j\theta}), \; H, \; H_{nom}, \; w, \; \Delta \in H^\infty, \; \|\Delta\|_\infty \leq 1 \right\} \qquad (21)$$

the formula for the MI rate presented here makes an assumption regarding the input signal $x(k)$, i.e., the input sequence $\{x(k)\}_{k \geq 0}$ is a discrete-time Gaussian stochastic process which is different from a standard positive IC input consisting of 0 and 1 s. Yet another problem is that 0 and 1 s are uniformly distributed. This is the reason we introduce an additional assumption and give further explanations. To ensure $x(k) \geq 0$, we assume that $x_i(k)$, $1 \leq i \leq r \leq p$ have mean values $a_i = E[x_i(k)] > 0$ such that $a_i = c\sigma_{x_i}$, $\sigma_{x_i}^2 = Var[x_i]$. In our case, we choose $c = 4$ ensuring 99.99% positive values for $x(k)$. Further, the application of the Gaussian input is justified by the fact that a Gaussian distribution gives a tight lower bound for the achievable rates subject to a discrete uniform input for low to moderate SNRs (see [29]). This means, that the Gaussian input provides a good estimation for the achievable rate for the uniform input in the case of low SNRs. A low SNR condition is true for new ICs since it is implied by a low power supply demand.

In [27], the achievable rate subject to variability in the transfer function matrix $H(e^{j\theta})$ described by (21) is given by

$$R_a \triangleq \max_{W_{\mathbf{x}} \in A_1} \min_{H \in A_2} J(W_{\mathbf{x}}, W_{\mathbf{n}}) \qquad (29)$$

where $J(W_{\mathbf{x}}, W_{\mathbf{n}})$ defined by

$$\frac{1}{4\pi} \int_0^{2\pi} \log \det(I_p + H(e^{j\theta})W_{\mathbf{x}}(\theta)H^H(e^{j\theta})W_{\mathbf{n}}^{-1}(\theta))d\theta \qquad (30)$$

is the MI rate between $\{x(k)\}_{k \geq 0}$ and $\{y(k)\}_{k \geq 0}$. $W_{\mathbf{n}}(\theta)$ is the PSD matrix of the noise $n(k)$. The solution of (29) is given by [27]

$$\max \quad \frac{1}{4\pi} \sum_{i=1}^{r} \int_0^{2\pi} \times \log\left(1 + \frac{W_{x_i}[(\sigma_i - |w|)^+]^2}{W_{n_i} + \sum_{k \neq i} |w|^2 W_{x_k}}\right)d\theta$$

$$\text{s.t.} \quad \sum_{i=1}^{r} \int_0^{2\pi} W_{x_i} d\theta = P_{\mathbf{x}}. \qquad (31)$$

Here, $W_{x_i}(\theta)$ and $W_{n_i}(\theta)$, $1 \leq i \leq r \leq p$, are diagonal entries of PSD matrices $W_x(\theta)$ and $W_n(\theta)$, respectively. $r \leq p$ is the number of nonzero singular values of $H_{\text{nom}}(e^{j\theta})$ or the rank of $H_{\text{nom}}(e^{j\theta})$. $\{\sigma_i(e^{j\theta})\}_{i=1}^{r}$ are the singular values of $H_{\text{nom}}(e^{j\theta})$. Without loss of generality, it is assumed that $W_{\mathbf{n}}(\theta)$ is diagonal. If this is not the case, then $W_{\mathbf{n}}(\theta)$ and $H(e^{j\theta})$ can jointly be treated as an equivalent channel assuming that the PSD of the noise is an identity matrix.

The formula for the achievable rate suggests that the bus can be decomposed into the r parallel channels along the singular values of the channel matrix $H_{\text{nom}}(e^{j\theta})$ as shown in Fig. 5. The transmission along each singular value is possible if $\sigma_i(e^{j\theta}) - |w(e^{j\theta})|$ is positive, which is denoted by a notation $(\cdot)^+$. $(\cdot)^+$ takes the value of an argument if the argument is positive; otherwise, it is zero. Hence, the size of the set A_2 (or the uncertainty set as it is often called), $|w(e^{j\theta})|$, determines how the achievable rate is affected by the uncertainty in the manufacturing process. The larger the uncertainty $|w(e^{j\theta})|$, the smaller the achievable rate R_a. If there is no uncertainty (the size of the uncertainty set $|w(e^{j\theta})|$ is zero), (31) reduces to the classical capacity of the
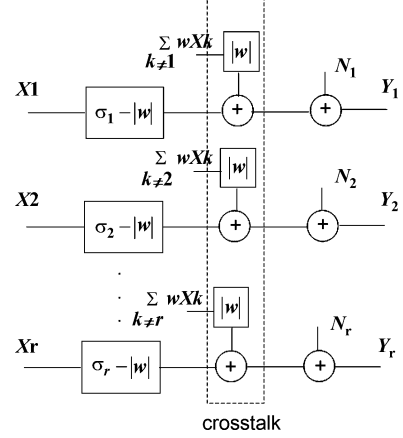

Fig. 5. Interpretation of R_a in terms of parallel channels.

MIMO communication channel [28]. If $\sigma_i(e^{j\theta}) < |w(e^{j\theta})|$, the ith channel disappears (see Fig. 5) because the ith channel coefficient becomes zero.

The formula for the achievable rate R_a given by (31) is interesting for other reasons as well. Notice that (31) is given in terms of the logarithm of the signal-to-noise ratio (SNR), i.e., $\log(1 + \text{SNR}_i(\theta))$, where

$$\text{SNR}_i(\theta) \triangleq \frac{W_{x_i}(\theta)(\sigma_i(e^{j\theta}) - |w(e^{j\theta})|)^2}{W_{n_i}(\theta) + \sum_{k \neq i} |w(e^{j\theta})|^2 W_{x_k}(\theta)}, \; 1 \leq i \leq r. \qquad (32)$$

The numerator is the power of the received useful signal at the ith interconnect, and the denominator is the equivalent noise consisting of the white noise W_{n_i} for the ith interconnect, and the crosstalk $\sum_{k \neq i} |w|^2 W_{x_k}$ from other interconnects as shown in Fig. 5. Therefore, it follows that the crosstalk noise is zero if there is no uncertainty. However, if there is uncertainty, the channel gain will be diminished $(\sigma_i - |w|)$, and, in the same time, the crosstalk noise will appear. In Section V, it will be demonstrated how it is possible to eliminate the crosstalk noise when there is no variability introduced by the manufacturing process.

Remark 4.1: How should (31) be interpreted? If the data transmission rate R is smaller than R_a, then there exists at least one encoding/decoding procedure (so called universal encoding/decoding) providing the probability of the decoding error arbitrarily close to zero regardless of the bus variability when the codeword length N becomes very large. In other words, the strength of the results stems from the fact that we can apply only one code for any bus that comes from the set A_2, and at the same time, we can guarantee the probability of the decoding error arbitrarily close to zero. This is the simplest and effective solution that one can have for this type of problems. The pros and cons of the approach employed here will be discussed in more detail in the next section.

Remark 4.2: Although the Gaussian input is the most optimal input for the Gaussian noise, we cannot claim that the signals on the IC have Gaussian distribution. Therefore, the future research should address the problem of computation of the achievable rates for the same channel model, but for different input distributions such as uniform.
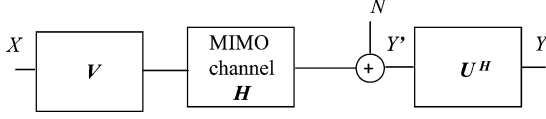
Fig. 6. Transmission scheme for uncertain channel matrix.

Remark 4.3: The unit of achievable rate given by (31) is bits per sample. Here, "sample" refers to the value of the signal taken at discrete-time moments which are T_s seconds apart. To get the achievable rate in bits per second, the value computed by (31) should be multiplied by $1/T_s$ samples/s.

V. ATTAINING ACHIEVABLE RATE

When a MIMO channel is known, an efficient communication is achieved by decomposing the MIMO channel into the r scalar independent, parallel channels, where r is the rank of the transfer function matrix. "Independent" means that there is no crosstalk among them. The idea is very simple; it consists of finding singular value decomposition of the transfer function matrix $H(e^{j\theta}) = U(e^{j\theta})\Sigma(e^{j\theta})V^H(e^{j\theta})$ and using unitary matrices $U(e^{j\theta})$ and $V(e^{j\theta})$ in processing the transmitted signal. Since, for the bus with variability we do not know the channel exactly, we apply the singular value decomposition on the nominal channel $H_{\text{nom}}(e^{j\theta}) = U(e^{j\theta})\Sigma(e^{j\theta})V^H(e^{j\theta})$. However, in this case the SVD does not produce independent parallel channels because of the uncertainty caused by variability. There will be some residual crosstalk that will be interpreted as an additional noise. Besides, the uncertainty will affect the channel coefficients, i.e., singular values, as explained in Section IV.

The strategy that attains the achievable rate (31) is the one that finds the worst-case communication channel representing the bus, and designs an encoder/decoder pair for this channel. The worst-case bus occurs when the channel coefficients, in terms of the singular values, take the smallest values for each frequency (the attenuation is the largest) and when the equivalent noise $N_{eq,i}(e^{j\theta})$ is the largest [see Section IV and (34)]. The reasoning behind this is the following: if the encoder and decoder performs well over the worst-case channel, it will perform even better over "better" channels, having larger channel coefficients and smaller noise. The rest of the section gives detailed description of the optimal communication scheme.

The communication scheme that attains achievable rate (31) is given in Figs. 6–8. First, the transmitted signal $x(k)$ is processed by the filter having the transfer function matrix $V(e^{j\theta})$ at the transmitter end of the bus (see Fig. 7), and processed by the filter $U^H(e^{j\theta})$ at its receiving end (see Fig. 8). $V_{li}(e^{j\theta})$, $1 \le l, i \le p$, are the entries of the lth row of $V(e^{j\theta})$, representing the scalar filters with impulse responses $v_{li}(k)$. $U_{li}(e^{j\theta})$, $1 \le l, i \le p$, are the entries of the lth row of $U(e^{j\theta})$, representing the scalar filters with impulse responses $u_{li}(k)$. Each encoder output $x_i(k)$, $1 \le i \le p$, is convolved with $v_{li}(k)$ to contribute to its bus input. At each bus output, received signal $y_l'(k)$ is convolved with $u_{il}^*(-k)$ to produce the lth output of the bus $y_l(k)$.

The matrices $U(e^{j\theta})$ and $V(e^{j\theta})$ can also be understood as a part of equivalent communication channel defined by
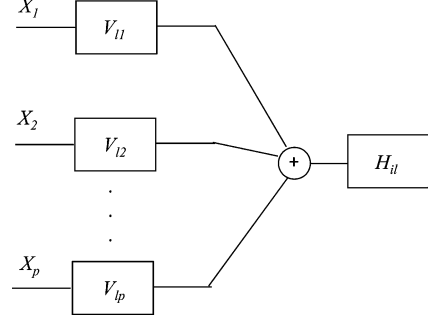

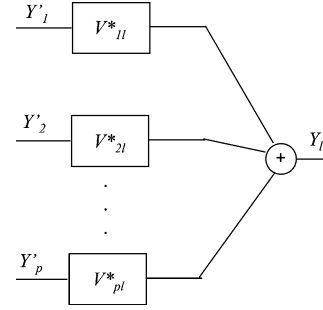Fig. 7. Signal processing at the transmitter's end of the bus.

Fig. 8. Signal processing at the receiver's end of the bus.

$U^H(e^{j\theta})H(e^{j\theta})V(e^{j\theta})$. Then, encoder/decoder pair sees the equivalent channel given by

$$
\begin{aligned}
H_{eq}(e^{j\theta}) &= U^H(e^{j\theta})H(e^{j\theta})V(e^{j\theta}) \\
&= \Sigma(e^{j\theta}) + U^H(e^{j\theta})\Delta(e^{j\theta})V(e^{j\theta})w(e^{j\theta}) \\
&= \Sigma(e^{j\theta}) + (\Delta_{s,\text{diag}}(e^{j\theta}) + \Delta_{s,\text{off-diag}}(e^{j\theta}))w(e^{j\theta})
\end{aligned}
$$

were $\Delta_s(e^{j\theta}) \triangleq U^H(e^{j\theta})\Delta(e^{j\theta})V(e^{j\theta})$, and $\Delta_s(e^{j\theta}) \triangleq \Delta_{s,\text{diag}}(e^{j\theta}) + \Delta_{s,\text{off-diag}}(e^{j\theta})$. $\Delta_{s,\text{diag}}(e^{j\theta})$ contains diagonal, while $\Delta_{s,\text{off-diag}}(e^{j\theta})$ contains off-diagonal entries of $\Delta_s(e^{j\theta})$, respectively. We can group further the first two terms, which are diagonal matrices, that determine the ith bus output as the function of the ith input solely. The third term is the crosstalk coming from the inputs different from the ith one. The output of the ith channel is represented in the frequency domain by

$$
\begin{aligned}
Y_i(e^{j\theta}) = &(\sigma_i(e^{j\theta}) + \delta_{s,ii}(e^{j\theta})w(e^{j\theta}))X_i(e^{j\theta}) \\
&+ \sum_{k \ne i} \delta_{s,ik}(e^{j\theta})w(e^{j\theta})X_k(e^{j\theta}) + N_i(e^{j\theta}). \quad (33)
\end{aligned}
$$

Here, $\delta_{s,li}(e^{j\theta})$, $1 \le l, i \le p$, are the entries of $\Delta_s(e^{j\theta})$. The off-diagonal elements $\delta_{s,li}(e^{j\theta})$, $l \ne i$, are absorbed into an equivalent noise

$$
N_{eq,i}(e^{j\theta}) = N_i(e^{j\theta}) + \sum_{k \ne i} \delta_{s,ik}(e^{j\theta})w(e^{j\theta})X_k(e^{j\theta}). \quad (34)
$$

Because $\|\Delta_s(e^{j\theta})\|_\infty \le 1$, it follows $|\delta_{s,li}(e^{j\theta})| \le 1$. From previous discussion, we can determine the worst-case communication channel representing the bus. The worst-case bus occurs when the channel coefficient $(\sigma_i(e^{j\theta}) + \delta_{s,ii}(e^{j\theta})w(e^{j\theta}))$ is the smallest for each frequency (the attenuation is the largest) and when the equivalent noise $N_{eq,i}(e^{j\theta})$ is the largest. This

will happen if $\delta_{s,ii}(e^{j\theta}) = e^{j\pi - j\phi_w}$ and $|\delta_{s,li}(e^{j\theta})| = 1, l \neq i$, where $w(e^{j\theta}) \triangleq |w(e^{j\theta})|e^{j\phi_w}$. Then, the channel coefficients become $\sigma_i(e^{j\theta}) - |w(e^{j\theta})|$, and the PSD of the noise is given by $W_{n_i}(\theta) + \sum_{k \neq i} |w(e^{j\theta})|^2 W_{x_k}(\theta)$. Thus, one can use r scalar error-correction codes, each tuned to the corresponding worst-case channel $\sigma_i(\theta) - |w(e^{j\theta})|$, and the equivalent noise. Since the codes work well for the worst case bus, it will work even better for other transfer function matrices from the set A_2.

Remark 5.1: There are a couple of practical questions that should be addressed when the suggested method is applied to deal with the crosstalk and uncertainty.

The first question is the choice of practical error-correcting codes that are going to be employed. This depends on system parameters such as delay. Since the encoding and decoding procedures introduce the delay, the designer would want to use short codes and low-complexity encoders and decoders in order to minimize overall system delay. However, we leave this question for future research.

The other question is related to the cost of applied filters in terms of power. From the point of view of information theory, in [28], it is shown that applied filters do not affect the received SNR. In other words, the performance of the overall communication system will not be tarnished by introducing filters U^H and $V(e^{j\theta})$.

VI. CASE-STUDY OF BUS ACHIEVABLE RATES

The following example illustrates the impact of different types of uncertainties on the achievable transmission rate. It is assumed that the bus consists of four parallel interconnects. Although, this is not usually the case, we choose $p = 4$ since for larger p, the achievable rate computation becomes more numerically involved, and the choice of p does not change the conclusions we want to deliver.

Next, it will be demonstrated how it is possible to construct the uncertainty set A_2 based on the introduced MIMO model and values for parasitic parameters. To compute the nominal matrix $H_{\text{nom}}(s)$, we take the values $\rho = 2.2 \times 10^{-8}$ Ωm, d, $w_w = 237 \times 10^{-9}$ m and t_1, $h = 498 \times 10^{-9}$ m, and use (10)–(17).

We also compute the transfer function matrices for three other scenarios: 1) $d = 237 \times 10^{-9} - 20\%$ m, $w_w = 237 \times 10^{-9} + 20\%$ m; 2) $d = 237 \times 10^{-9} - 10\%$ m; $w_w = 237 \times 10^{-9} + 10\%$ m and $\rho = 2.2 \times 10^{-8} + 15\%$ Ωm; and 3) $t_1 = 498 \times 10^{-9} - 10\%$ m.

Denote the bus transfer function matrices for previous three scenarios by $H_c(s)$, $H_{rc}(s)$, and $H_e(s)$, respectively. They are going to be used to construct three examples of uncertainty sets A_2.

In the simulations, we use $L = 12$ μm and the relative permittivity of $\epsilon_r = 3.9$ [16].

Fig. 19 summarizes all parameters of transfer functions (tf) used in the case-study.

In all three scenarios, we take into account correlation among bus parameters. Scenario 1 shows the case when the space between two interconnects of the bus is smaller than the nominal, implying that the interconnect width is larger than the nominal. This uncertainty leads to the increase of C_g and C_c and decrease in R_w.
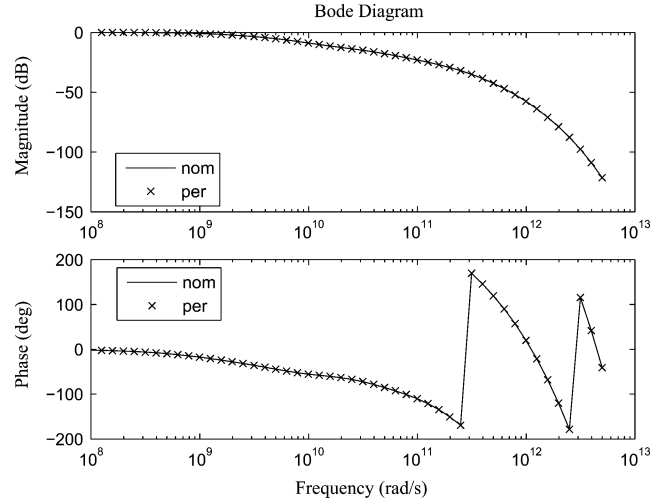

Fig. 9. Bode plots of the nominal bus and the bus with larger than nominal C_g and C_c capacitances having length of 400 sections [(1,1) entries of transfer function matrices].

Scenario 2, in addition to previous assumptions, treats the case when the resistivity ρ is larger by 15%. The main reason for the resistivity uncertainty is that the metal used for interconnect is not a pure material, but a compound with the main base of copper or aluminum. It is further surrounded by another thin layer as the barrier layer. The overall resistivity is the average of all these materials. Further, as the wire size is scaled down getting close to a metal grain size, the deposition process itself becomes harder to control. That is another reason causing a random variation of the resistivity. This uncertainty leads to the increase of all three bus parasitic parameters.

Scenario 3 simulates the erosion illustrated by Fig. 3. This uncertainty leads to the increase of R_w and decrease of C_c.

Figs. 9, 11, and 13 show the Bode plots of (1,1) entries of the $H_c(s)$, $H_{rc}(s)$, and $H_e(s)$, respectively, each accompanied with (1,1) entry of the $H_{\text{nom}}(s)$, where $s \triangleq j\omega$. It can be seen that $H_{rc}(s)$ and $H_e(s)$ introduce larger attenuation comparing to $H_{\text{nom}}(s)$. The same behavior is observed for all other diagonal entries of $H_{rc}(s)$ and $H_e(s)$ that describe how the ith entry affects the ith output of the bus. Further, Figs. 12 and 14 illustrate a typical characteristic of off-diagonal entries of $H_{rc}(s)$ and $H_e(s)$. Namely, off-diagonal entries of $H_{rc}(s)$ and $H_e(s)$ experience larger crosstalk than $H_{\text{nom}}(s)$. On the other hand, Figs. 9 and 10 show that the transfer function matrix $H_c(s)$ is almost identical with the nominal $H_{\text{nom}}(s)$. This can be understood by noticing that the scenario 1 has opposite effects on the parasitic parameters; although C_g and C_c are increased, R_w is decreased.

The previous analysis suggests that it is very important to take into account the correlation of bus parameters when considering the effect of the uncertainty on the bus performance. Also, it can be seen that the resistivity can play a major role in defining the bus performance subject to the uncertainty.

Further, we are going to deal with the 60-section-long bus, and all transfer functions refer to that particular bus. To obtain the transfer function matrices that correspond to discrete-time domain, denoted by $H_{rc}(z)$, $H_e(z)$, and $H_{\text{nom}}(z)$ (switching
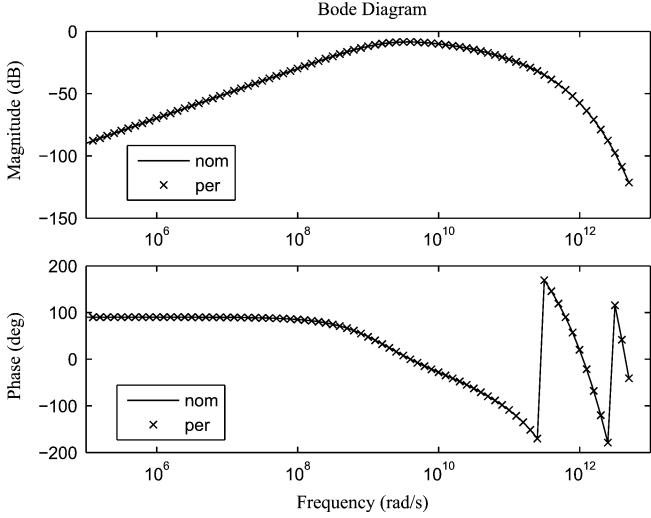
Fig. 10. Bode plots of the nominal bus and the bus with larger than nominal C_g and C_c capacitances having length of 400 sections [(1,2) entries of transfer function matrices].
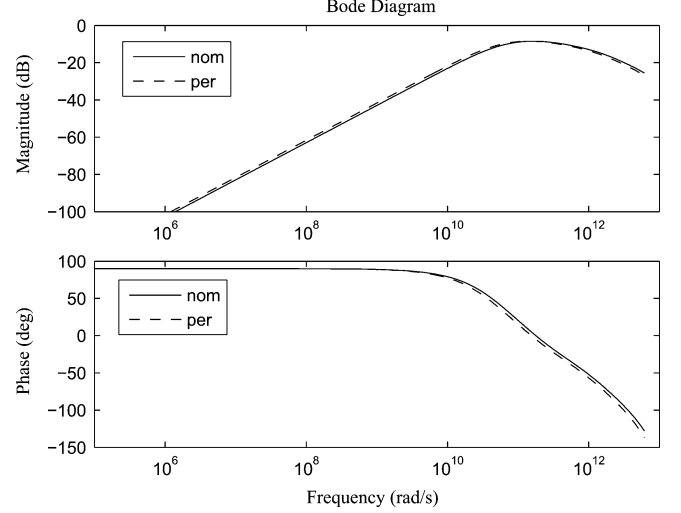

Fig. 12. Bode plots of the nominal bus and the bus with larger than nominal resistivity ρ having length of 60 sections [(1,2) entries of transfer function matrices].
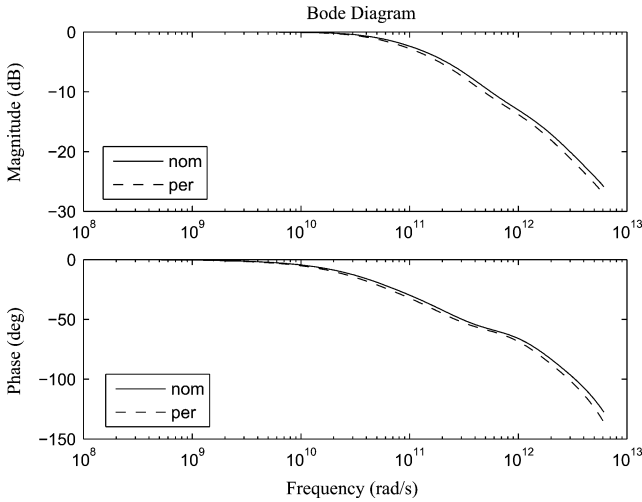

Fig. 11. Bode plots of the nominal bus and the bus with larger than nominal resistivity ρ having length of 60 sections [(1,1) entries of transfer function matrices].
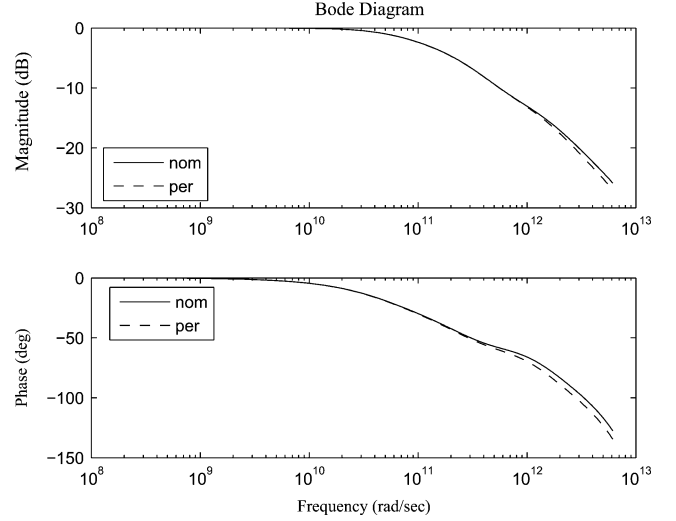

Fig. 13. Bode plots of the nominal bus and the bus subject to erosion having length of 60 sections [(1,1) entries of transfer function matrices].

from Laplace transform to Z transform), Tustin discretization of the continuous-time transfer function matrices $H_{rc}(s)$, $H_e(s)$, and $H_{nom}(s)$, is carried out. The output of the system is sampled with the sampling interval $T_s = 10^{-12}$ s. This sampling interval has been chosen since from Fig. 11, it can be noticed that attenuation of 10 dB is achieved between $\omega = 10^{11}$ rad/s and $\omega = 10^{12}$ rad/s.

The frequency response matrix from $H(z)$ is generated by substituting z with $e^{j\omega T_s} = e^{j\theta}$. When $-\omega_N \leq \omega \leq \omega_N \triangleq \pi/T_s$, then $-\pi \leq \theta \leq \pi$, where ω_N is the Nyquist frequency.

Now, the uncertainty set is constructed in the following way. To ensure that $H_{rc}(z)$ belongs to the uncertainty set A_2, observe that

$$\bar{\sigma}(H_{rc}(e^{j\theta}) - H_{nom}(e^{j\theta})) = \bar{\sigma}(\Delta(e^{j\theta})w(e^{j\theta})) \leq |w(e^{j\theta})|.$$

It is chosen that the size of the uncertainty set $|w(e^{j\theta})|$ is equal to $\bar{\sigma}(H_{rc}(e^{j\theta}) - H_{nom}(e^{j\theta}))$ for each frequency $-\pi \leq \theta \leq \pi$, thus to its lower bound, which represents the distance from the nominal channel transfer matrix $H_{nom}(e^{j\theta})$ to the worst-case matrix $H_{rc}(e^{j\theta})$. Fig. 15 shows the frequency dependence of the singular values of $H_{nom}(e^{j\theta})$ accompanied with the size of uncertainty set $|w(e^{j\theta})|$. In fact, Fig. 15 depicts the magnitudes of two transfer functions $w_1(e^{j\theta})$ and $w_2(e^{j\theta})$ that correspond to the uncertainty sets constructed around $H_{rc}(e^{j\theta})$ and $H_e(e^{j\theta})$, respectively. For all frequencies $|w_1(e^{j\theta})| \geq |w_2(e^{j\theta})|$ demonstrating the larger distance from $H_{nom}(e^{j\theta})$ to $H_{rc}(e^{j\theta})$ than from $H_{nom}(e^{j\theta})$ to $H_e(e^{j\theta})$. The loss of achievable data rate due to the uncertainty can be anticipated by observing that the achievable rate depends on the difference between the singular values of $H_{nom}(e^{j\theta})$ and the magnitude of the uncertainty set $w(e^{j\theta})$. The contribution of each frequency to the achievable rate is measured by this
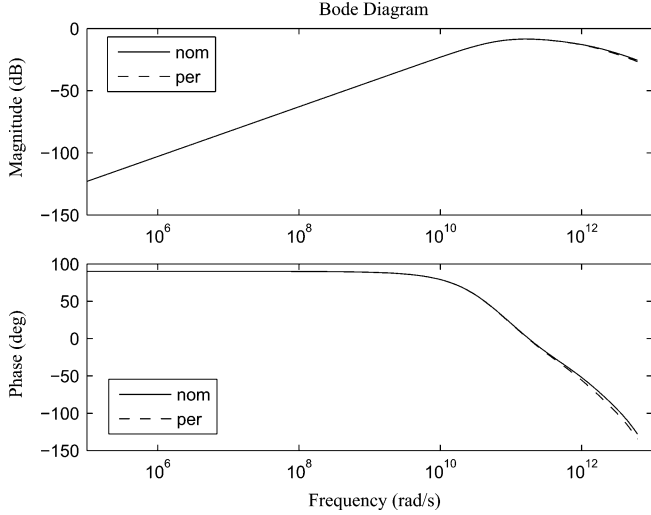
Fig. 14. Bode plots of the nominal bus and the bus subject to erosion having length of 60 sections [(1,2) entries of transfer function matrices].
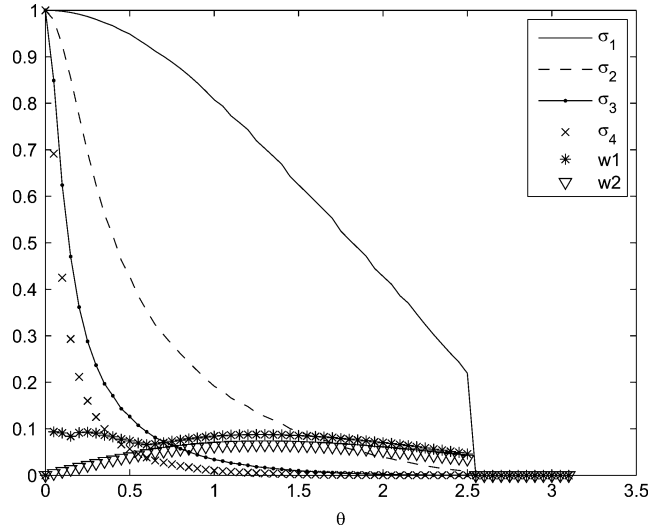

Fig. 16. Impulse responses of the nominal and perturbed buses.

Fig. 15. Singular values of H_{nom} and the sizes of uncertainty sets versus frequency θ.
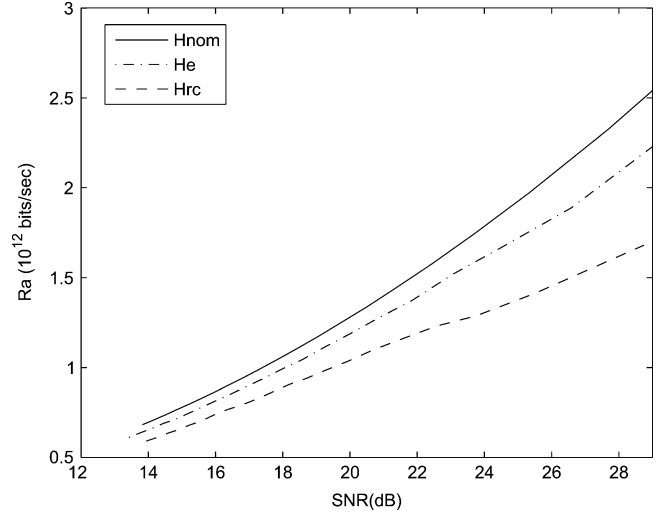
Fig. 17. Achievable rates for nominal bus and two CBs.

difference. If for some frequency $\sigma_i(\theta) - |w(e^{j\theta})| < 0$, the contribution of this frequency is zero.

Fig. 16 shows the impulse responses of $\sigma_i(\theta)$, $\sigma_i(\theta) - |w_1(e^{j\theta})|$ and $\sigma_i(\theta) - |w_1(e^{j\theta})|$ $1 \leq i \leq 4$, which correspond to the equivalent channel representation for $H_{\text{nom}}(e^{j\theta})$, $H_{rc}(e^{j\theta})$, and $H_e(e^{j\theta})$. A main observation is that the uncertainty reduces the amplitude of the impulse response in the vicinity of $k = 0$ and broadens the impulse response for higher values of k. This affects the reliability of the transmission in two ways: 1) due to the lower amplitude of the impulse response in the vicinity of $k = 0$, the decision about the sent bit at $k = 0$ is more sensitive to the additive noise and 2) broaden impulse response introduces larger inter-symbol interference for subsequent bits making the decision regarding these bits less reliable (see Fig. 2). Therefore, to improve the performance, a communication technique for suppressing inter-symbol interference has to be employed.
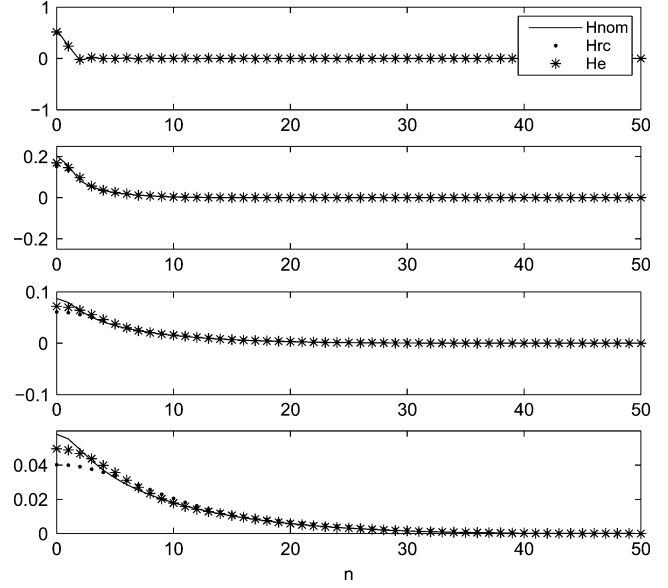
In Fig. 17, the achievable rates are plotted for the nominal channel, and for the CBs when the worst-case channel matrices are determined by $H_{rc}(e^{j\theta})$ and $H_e(e^{j\theta})$, respectively. The noise PSD matrix $W_{\mathbf{n}}(\theta)$ is taken to be diagonal with diagonal entries being equal and equal to 0.04 that make sense for the power supply of $V_{\text{DD}} = 2$ V. The plots reveal noticeable reduction in the achievable rates when the uncertainty is determined by the variation in the resistivity ρ. For instance, for SNR $= 17.85$ dB, the achievable rate for the nominal channel is $R_a = 1.045 \times 10^{12}$ bit/s, while for the $H_{rc}(e^{j\theta})$ based CB is $R_a = 0.85 \times 10^{12}$ bit/s which corresponds to 15% loss. For SNR $= 20$ dB, the achievable rate for the nominal channel is $R_a = 1.3 \times 10^{12}$ bit/s, while for the $H_{rc}(e^{j\theta})$ based CB is $R_a = 1.04 \times 10^{12}$ bit/s corresponding to 23% loss.

Remark 6.1: The example reveals the weakness of universal encoding approach. If only one universal code is to be used, the price has to be paid in terms of the reduced achievable rate. Another alternative approach for NOC advocated in [3] is the

symbol	meaning
$x(k)$	bus input signal
$y(k)$	bus output signal
$h(k)$	impulse response
$n(k)$	additive noise
P	power constraint
R_a	achievable code rate
R	code rate
T_s	sampling interval
H_{nom}	nominal transfer function
$w(e^{j\theta})$	size of uncertainty set
σ_i	singular value of matrix H_{nom}
ρ	metal resistivity
w_w	wire width
d	separation between bus lines
t_1	wire height
h	height of wire above substrate
ε	permittivity of oxide between wires
L	length of bus
R_w	wire resistance
C_g	wire-to-substrate capacitance
C_c	coupling capacitance

Fig. 18. Notations and parameter definitions.

tf	parameters
$H_{nom}(s)$	$d, w_w = 237\text{nm}, t_1, h = 498\text{nm}, \rho = 22\text{n}\Omega\text{m}$
$H_c(s)$	$d = 237\text{nm} - 20\%, w_w = 237\text{nm} + 20\%$
$H_{rc}(s)$	$d = 237\text{nm} - 10\%, w_w = 237\text{nm} + 10\%, \rho = 22\text{n}\Omega\text{m} + 15\%$
$H_e(s)$	$t_1 = 498\text{nm} - 10\%$

Fig. 19. Parameters of transfer functions.

use of feedback and automatic-repeat-request (ARQ) schemes. However, this requires some kind of adaptivity of the encoding procedure and complex decoding techniques since the channel is not precisely known. Consequently, everything boils down to what price one wishes to pay. Universal codes offer low complexity but reduced achievable rate, while ARQ could give higher achievable rate with increased complexity. At the end, one might explore combinations of both techniques in addition to manufacturing technology improvement to find an optimal solution.

Remark 6.2: As pointed out in Section IV, (31) includes the term describing the crosstalk noise. In Fig. 17, SNR is defined as

$$10\log_{10} \frac{P}{\frac{1}{2\pi}\int_0^{2\pi} Trace(W_{\mathbf{n}}(\theta))d\theta} \tag{35}$$

where $W_{\mathbf{n}}(\theta)$ is primarily concerned with the thermal noise and other noises which arise in electronic circuits excluding the crosstalk noise. Thus, overall SNR will actually be smaller.

VII. ERROR CORRECTION CODES FOR CB

Consider the case of the bus consisting of 4 parallel interconnects which has been discussed earlier. The choice of error correcting codes is constrained by a number of factors, foremost of which is the achievable data rate that upper bounds the rate of the codes for achieving error free transmission over the bus. For example, Fig. 17 suggests that between 12 and 14 dB, the achievable data rate is around 0.5×10^{12} bit/s. Here, we are going to assume that this rate is equally divided to four scalar error correcting codes, each operating on one line of the

bus. Actually, the encoders and decoders operate on the equivalent channel shown in Fig. 6 which includes filters V and U^H. Therefore, a code rate for each code should not be larger than $0.5/4 = 0.125$. One possible choice for the codes would be a (63,7) Euclidian Geometry codes [30], whose code rate is $7/63 = 0.111 < 0.125$.

The choice of codes is also limited by complexity, delay and power requirements, which often require the codes to have conflicting characteristics. For instance, codes with longer lengths usually achieve better performance but at the cost of higher latency and decoder complexity. In the following discussion, we attempt to point out several examples of codes and decoders with varied implementation complexities, which could be good candidates for the CB.

For this high-speed application, it is generally suitable to use codes of very small length to reduce latency and decoder complexity. There exist numerous decoders that range from very-low complexity to high complexity, whose performances are usually proportional to their complexity. In general, decoders can be classified as low-complexity hard-decoders and high-complexity soft-decoder. Among the simplest decoders are one-step and multistep majority logic decoders (MLD) [30], [31], which usually require only a few logic gates to implement. These decoders are ideal candidates for extremely high-speed applications that can be operated at 10–40 Gb/s, though their performance pales in comparison to more sophisticated decoding algorithms. Many well-known algebraic codes like BCH, Reed–Muller codes and codes from finite geometries can be decoded using such decoders [30]. The hardware circuitry for these codes consists of a set of multi-input XOR and multi-input majority-logic gates. For example, a one-step MLD for a (15,7) BCH code requires only four four-input XOR gates, a four-input majority logic gate, and a 15-bit shift-register. Multi-step MLD performs better than one-step MLD but are marginally more complex. A two-step MLD for a (15,5) BCH code requires only 36 four-input XOR gates, seven six-input majority-logic gates, and a 15-bit shift register. There are many low-rate very short codes that can be used with this class of decoders.

Soft-decoders that make use of soft-values perform better than hard-decoders by many orders of magnitude, but require far more complex circuitry. Best performance for any code is achieved by the optimal maximum *a posteriori* (MAP) decoder [30]. Normally, it is impractical to implement this algorithm for most codes. But it is possible to implement it for certain very short codes. In [32], MAP decoder for a (8,4) Hamming code is implemented on a 0.5 μm CMOS technology with a decoder circuit size of 0.82 mm^2. Bit-rates at 2–10 Mb/s are significantly lower than what is capable with hard-decoders. The most important class of soft-decoders is the class of iterative decoders, which are suboptimal, but of relatively lower complexity than MAP decoders. Some of the best performances reported so far are due to such decoders applied to a class of codes called low-density parity-check (LDPC) codes. In [33], an iterative decoder for a (32,8) LDPC code is implemented on a 0.18μm CMOS technology requiring a core area of 0.57 mm^2 with a throughput of 6 Mb/s. For 65-nm CMOS technology, the

LDPC code implementation has 690 mW as power dissipation, 1 Gb/s as speed and 0.25 mm^2 as the area based on values from [34].

Finally, the overall complexity of the scheme also depends on the encoder/decoder architecture over the bus lines. For instance, the data through the bus lines may be transmitted by independently encoding and decoding data in each bus line. Alternately, a single stream of input data may be encoded and transmitted by equally distributing over all four bus lines. Other variations over this architecture are also possible. Again, the type of architecture to be used is determined by the specific system requirements.

VIII. Conclusion

New VLSI manufacturing processes inevitably introduce IC interconnect variability. This paper considers several different key issues such as: 1) modeling interconnect variability; 2) measuring the variability effect on the interconnect performance; and 3) proposing possible design solutions based on the Information Theory concepts. We suggest frequency-domain variability modeling by using H^∞ space norm. For this model, the achievable data transmission rate is computed, and encoding/decoding strategy is proposed that guarantees the reliable transmission of information along the bus interconnects regardless of their variability. We identified several problems such as intersymbol interference and encoder/decoder complexity that should be studied in the future research.

Appendix

To introduce the H^∞ space and $\|\cdot\|_\infty$ norm, we need the notions of transfer function stability.

A transfer function $H(z)$ is called stable if and only if all its poles lie within the unit circle in the z complex plain. If $H(z)$ is a matrix transfer function, $H(z)$ is stable if and only if all its entries are stable [26].

The H^∞ space is the set of all stable transfer function matrices.

The H^∞ norm of the system given by the matrix $H(e^{j\theta})$ ($\|H\|_\infty$) is computed as

$$\|H\|_\infty \triangleq \sup_{\theta \in [0,2\pi)} \bar{\sigma}[H(e^{j\theta})] \qquad (36)$$

where $\bar{\sigma}[H(e^{j\theta})]$ denotes the maximum singular value of the matrix $H(e^{j\theta})$. In the case of the scalar $H(e^{j\theta})$, (36) reduces to

$$\|H\|_\infty \triangleq \sup_{\theta \in [0,2\pi)} |H(e^{j\theta})| \qquad (37)$$

i.e., to the peak of the magnitude of the Bode plot of $H(e^{j\theta})$.

References

[1] ITRS, "The International Technology Roadmap for Semiconductors," 2005. [Online]. Available: http://www.itrs.net

[2] I. Bahar, J. Harlow, D. Hammerstrom, W. Joyner, C. Lau, D. Marculescu, A. Orailoglu, and M. Pedram, "Executive summary: Architectures for silicon nanoelectronics and beyond," presented at the NSF Nanoarchitecture Workshop, Portland, OR, 2005.

[3] V. Raghunathant, M. B. Srivastavat, and R. K. Guptai, "A survey of techniques for energy efficient on-chip communication," in *Proc. DAC*, Anaheim, CA, Jun. 2003, pp. 900–905.

[4] Y. Cao, P. Gupta, A. B. Kahng, D. Sylvester, and J. Yang, "Design sensitivities to variability: Extrapolations and assessments in nanometer VLSI," in *Proc. ASIC/SOC Conf.*, Sep. 2002, pp. 411–415.

[5] J. Cong, L. He, C. K. Koh, and Z. Pan, "Interconnect sizing and spacing with consideration of coupling capacitance," *IEEE Trans. Comput.-Aided Des. Integr. Circuits Syst.*, vol. 20, no. 9, pp. 1164–1169, Sep. 2001.

[6] J. Cong, C. K. Koh, and P. H. Madden, "Interconnect layout optimization under higher order RLC model fo MCM designs," *IEEE Trans. Comput.-Aided Des. Integr. Circuits Syst.*, vol. 20, no. 12, pp. 1455–1463, Dec. 2001.

[7] J. Cong, T. Kong, and Z. Pan, "Buffer block planning for interconnect planning and prediction," *IEEE Trans. Very Large Scale Integr. (VLSI) Syst.*, vol. 9, no. 6, pp. 929–937, Dec. 2001.

[8] C. J. Alpert, J. Hu, S. S. Sapatnekar, and P. G. Villarrubia, "A practical methodology for early buffer and wire resource allocation," in *Proc. DAC*, Las Vegas, NE, Jun. 2001, pp. 189–194.

[9] C. J. Alpert, C. Chu, G. Gandham, M. Hrkic, J. H. C. Kashyap, and S. T. Quay, "Simultaneous driver sizing and buffer insertion using a delay penalty estimation technique," *IEEE Trans. Comput.-Aided Des. Integr. Circuits Syst.*, vol. 23, no. 1, pp. 136–141, Jan. 2004.

[10] H. Su, J. Hu, S. S. Sapatnekar, and S. R. Nassif, "A methodology for the simultaneous design of supply and signal networks," *IEEE Trans. Comput.-Aided Des. Integr. Circuits Syst.*, vol. 23, no. 12, pp. 1614–1624, Dec. 2004.

[11] P. Yu and D. Z. Pan, "TIP-OPC: A new topological invariant paradigm for pixel based optical proximity correction," in *Proc. IEEE ACM Int. Conf. Comput.-Aided Des. (ICCAD)*, San Jose, CA, Nov. 2007, pp. 847–853.

[12] P. Yu and D. Z. Pan, "Novel intensity based OPC algorithm with speedup in lithography simulation," in *Proc. IEEE ACM Int. Conf. Comput.-Aided Des. (ICCAD)*, San Jose, CA, Nov. 2007, pp. 854–859.

[13] L. Scheffer, "On-chip interconnect variation," 2005. [Online]. Available: http://sliponline.org/SLIP06/Presentations/2_1_lou.pdf

[14] S. R. Sridhara and N. R. Shanbhag, "Coding for system on chip networks: A unified framework," *IEEE Trans. Very Large Scale Integr. (VLSI) Syst.*, vol. 13, no. 6, pp. 655–667, Jun. 2005.

[15] M. Favalli and C. Metra, "Bus crosstalk fault-detection capabilities of error-detecting codes for on-line testing," *IEEE Trans. Very Large Scale Integr. (VLSI) Syst.*, vol. 7, no. 3, pp. 392–396, Sep. 1999.

[16] R. Singhal, G. S. Choi, and R. Mahapatra, "Information theoretic capacity of long on-chip interconnects in the presence of crosstalk," in *Proc. 7th Int. Symp. Quality Electron. Des. (ISQED)*, San Jose, CA, 2006, pp. 407–412.

[17] K. N. Patel and I. L. Markov, "Error-correction and crosstalk avoidance in dsm busses," *IEEE Trans. Very Large Scale Integr. (VLSI) Syst.*, vol. 12, no. 10, pp. 1076–1080, Oct. 2004.

[18] D. Bertozzi, L. Benini, and B. Ricco, "Energy-efficient and reliable low-swing signaling for on-chip buses based on redundant coding," in *Proc. IEEE ISCAS*, 2002, vol. 1, pp. 93–96.

[19] Y. M. Chee, C. J. Colbourn, and A. C. H. Ling, "Optimal memoryless encoding for low power off-chip data buses," in *Proc. IEEE ICCAD*, Nov. 2006, pp. 369–374.

[20] R. R. Rao, H. S. Deogun, D. Blaauw, and D. Sylvester, "Bus encoding for total power reduction using a leakage-aware buffer configuration," *IEEE Trans. Very Large Scale Integr. (VLSI) Syst.*, vol. 13, no. 12, pp. 1376–1383, Dec. 2005.

[21] R. Hedge and N. R. Shanbhag, "Toward achieving energy efficiency in presence of deep submicron noise," *IEEE Trans. Very Large Scale Integr. (VLSI) Syst.*, vol. 8, no. 4, pp. 379–390, Aug. 2000.

[22] S. R. Sridhara, A. Ahmed, and N. R. Shanbhag, "Area and energy-efficient crosstalk avoidance codes for on-chip buses," in *Proc. ICCD*, San Jose, CA, 2004, pp. 12–17.

[23] C. E. Shanon, "A mathematical theory of communication," *Bell Syst. Tech. J.*, vol. 27, pp. 623–656, 1948.

[24] A. Lapidoth and P. Narayan, "Reliable communication under channel uncertainty," *IEEE Trans. Inf. Theory*, vol. 44, no. 10, pp. 2148–2177, Oct. 1998.

[25] W. L. Root and P. P. Varaiya, "Capacity of classes of Gaussian channels," *SIAM J. Appl. Math.*, vol. 16, no. 6, pp. 1350–1393, Nov. 1968.

[26] J. Doyle, B. Francis, and A. Tannenbaum, *Feedback Control Theory*. New York: Macmillan, 1992.

[27] S. Z. Denic, "Communication subject to normed channel uncertainty," Ph.D. dissertation, Sch. Inf. Technol. Eng.,, Univ. Ottawa, Ottawa, ON, Canada, 2006.

[28] E. Telatar, "Capacity of multi-antenna Gaussian channels," *Eur. Trans. Telecomm.*, vol. 6, no. 10, pp. 585–596, Nov. 1999.

[29] S. Denic, I. Djordjevic, J. Anguita, B. Vasic, and M. Neifeld, "Information theoretic limits for free-space optical channels with and without memory," *IEEE J. Light Wave Technol.*.

[30] S. Lin and D. J. Costello, *Error Control Coding*. Englewood Cliffs, NJ: Prentice-Hall, 1983, pp. 273–290.

[31] I. S. Reed, "A class of multiple-error correcting codes and the decoding of scheme," *IRE Trans.*, vol. 4, pp. 38–49, Sep. 1954.

[32] C. Winstead, J. Dai, S. Yu, C. Myers, R. R. Harrison, and C. Schlegel, "CMOS analog MAP decoder for (8,4) Hamming code," *IEEE J. Solid-State Circuits*, vol. 39, no. 1, pp. 122–131, Jan. 2004.

[33] S. Hemati, A. H. Banihashemi, and C. Plett, "A 0.18-μm CMOS analog min-sum iterative decoder for a (32,8) low-density parity-check (LDPC) code," *IEEE J. Solid-State Cir.*, vol. 41, no. 11, pp. 2531–2540, Nov. 2006.

[34] A. J. Blanksby and C. J. Howland, "A 690 mW 1 Gb/s 1024-b, rate-1/2 low-density parity-check codedecoder," *IEEE J. Solid-State Circuits*, vol. 37, no. 3, pp. 404–412, Mar. 2002.

Stojan Z. Denic (S'04–M'06) received the B.Sc. and M.Sc. degrees in electrical engineering from the Faculty of Electronic Engineering, University of Nis, Nis, Serbia, in 1994 and 2001, respectively, and the Ph.D. degree in electrical engineering from the School of Information Technology and Engineering, University of Ottawa, Ottawa, ON, Canada, in 2006.

He currently holds a Senior Research Engineer post with the Telecommunications Research Laboratory, Toshiba Research Europe Limited, Bristol, U.K. From 1994 to 1996, he was a Research Assistant with the Telecommunications Lab, the Faculty of Electronic Engineering, University of Nis, Nis, Serbia. In 1996, he joined Telekom Srbija, Serbia, as a Network Design Engineer. From 2000 to 2006, he was a graduate student with the School of Information Technology and Engineering, University of Ottawa, Ottawa, ON, Canada. In the meantime, from 2005 to 2006, he was visiting the Department of Electrical and Computer Engineering, University of Cyprus, Nicosia, Cyprus. In 2006, he joined the Department of Electrical and Computer Engineering, University of Arizona, Tucson, where he was a Research Assistant Professor until 2008. His research interests include information theory, communication over uncertain channels, control over communication channels, optical communications, and coding for wireless and digital recording channels.

Bane Vasic (S'92–M'93–SM'02) received the B.Sc., M.Sc., and Ph.D. degrees in electrical engineering from the University of Nis, Nis, Serbia, in 1989, 1991, and 1994, respectively.

Currently, he is a Professor with the Department of Electrical and Computer Engineering and Mathematics, University of Arizona, Tucson. Prior to this appointment, he was at Bell Laboratories, Allentown, PA. He authored a number of journal and conference articles and book chapters, and edited two books. His patents are implemented in Bell Lab chips. His research interests include coding theory, communication theory, constrained systems, and digital communications and recording.

Dr. Vasic is a Member of the Editorial Board of the IEEE TRANSACTIONS ON MAGNETICS, and was a Chair or Technical Program Chair for several workshops and conferences including 2003 and 2007 IEEE Communication Theory Workshop (CTW); 2004 DIMACS Workgroup and Workshop on Theoretical Advances in Information Recording; 2004 LANL Workshop on Applications of Statistical Physics to Coding Theory; and 2006 Communication Theory Symposium within ICC.

Charalambos D. Charalambous (S'90–M'91–SM'05) received the B.S., M.E., and Ph.D. degrees from Old Dominion University, Norfolk, VA, in 1987, 1988, and 1992, respectively, all in electrical engineering.

In 2003, he joined the Department of Electrical and Computer Engineering, University of Cyprus, Nicosia, Cyprus, where he is currently an Associate Professor. In 2005, he was elected Associate Dean of the School of Engineering for a three-year term. He was an Associate Professor with University of Ottawa, School of Information Technology and Engineering from 1999 to 2003, and an Adjunct Professor with McGill University from 1999 to 2002. He has served on the faculty of McGill University, Department of Electrical and Computer Engineering, as a visiting faculty, from 1995 to 1999. From 1993 to 1995, he was a Post-Doctoral Fellow with Idaho State University, Engineering Department. His current research interests are in theory and applications of stochastic processes and systems subject to uncertainty, communication and control systems, large deviations, information theory, and connections between robustness, information theory, and statistical mechanics.

Dr. Charalambous is currently an Associate Editor of the IEEE COMMUNICATIONS LETTERS, *Systems and Control Letters*, and from 2002 to 2004 he served as an Associate Editor of the IEEE TRANSACTIONS ON AUTOMATIC CONTROL. He was a member of the Canadian Centers of Excellence through MIT ACS. (the mathematics of information technology and complex systems), from 1998 to 2001. In 2001, he received the Premier's Research Excellence Award of the Ontario Province of Canada.

Jifeng Chen (S'08) received the B.S. and M.S. degrees in the area of telecommunications engineering from the Xidian Unversity, China, in 2002 and 2006, respectively, and the M.S. degree in computer engineering from the University of Arizona, Tucson, in 2009.

His current research interests mainly include the high-speed interconnect, transceiver and receiver design and modeling for nanoscale circuits under submicron technologies.

Janet M. Wang (M'98–SM'08) received the B.S. degree from Nanjing University of Science and Technology (former East China Institute of Technology), Nanjing, China, in 1991, the M.E. degree from the Chinese Academy of Sciences, Beijing, China, in 1994, and the M.S. and Ph.D. degrees in electrical engineering and computer sciences from the University of California, Berkeley, in 1997 and 2000, respectively.

She was with Intel, Santa Clara, CA, and Cadence, Santa Clara, CA, from 2000 to 2002. Since 2003, she has been a Faculty Member in the Electrical Computing Engineering Department, University of Arizona, Tucson.

Dr. Wang is a member of the IEEE Circuits and Systems Society. She was a recipient of the 2005 National Science Foundation Career Award and 2006 Presidential Early Career Award for Scientists and Engineers.